Editors' Suggestion

Self-propulsion of a helical swimmer in granular matter

Rogelio Valdés, Verónica Angeles, Elsa de la Calleja, and Roberto Zenit*
Instituto de Investigaciones en Materiales, Universidad Nacional Autónoma de México, Apartado Postal 70-360, Ciudad Universitaria, Distrito Federal 04510, México

(Received 16 December 2018; published 13 August 2019)

The motion of helicoidal swimmers moving in a pool filled with a granular medium is studied experimentally. The horizontal displacement through granular beads is measured considering geometrical modifications of the swimmer, the size, and frictional properties of the media. We found three main parameters which affect the swimming performance: the diameter, the wavelength, and the angle of the helix. The swimming speed scales with the rotation speed, ωR. The size of particles does not affect the swimming speed significantly; the swimming speed is reduced when the particle's angle of repose increases. It was found that a maximum swimming speed is achieved when the helix angle is close to 55°. The experimental data are compared with predictions of the granular resistive force theory, which was extended to be applicable for a swimmer with a rigid helical tail, leading to good agreement.

DOI: 10.1103/PhysRevFluids.4.084302

I. INTRODUCTION

The locomotion of living organisms has been extensively studied in the fluid mechanics community for centuries [1]. The interaction of moving body parts and a fluid environment gives rise to both thrust and drag forces which, under the correct conditions, produce locomotion. While flying and swimming (both at low and large Reynolds numbers) are well understood for the case of Newtonian fluids [2], locomotion in more complex media has not been studied extensively and, in consequence, remains poorly understood. In particular, digging through granular materials is a frequently observed strategy in nature [3]: it is used by many animals to feed, move, and escape predators. The challenge to understand motion in such complex media is that granular matter can behave in significantly different manners, as a solid or as a fluid [4], even in the same flow. Therefore, a general constitutive equation does not exist. There have been significant recent advances, in particular for the case of dense granular flows [5,6]; however, wide acceptance and validation are still needed.

Locomotion in granular media has drawn significant attention by the community. Goldman and collaborators, in a series of seminal contributions [7–12], have studied the undulatory motion of organisms in sand, such as the sandfish lizard (*Scincus scincus*). Using a state-of-the-art x-ray camera, they were able to visualize the motion of the lizard as it burrowed itself into a bed of particles. The organism performed a very distinct motion: while displacing into sand, it moved in a sideways undulatory motion with constant frequency and amplitude. With these observations they conjectured that the motion resembled that of microorganisms at low Reynolds numbers. Hence, they took the classical resistive force theory (RFT) for low Reynolds locomotion [13] and adapted it to be compatible with the physics of granular matter [7]. They found good agreement between the observations and the predictions of the granular resistive force theory [8]. However, further

*zenit@unam.mx

validation of the theory could not be tested in the biological case because the organisms could not be made to change their swimming strategy.

Following these studies, more recent investigations have addressed the other related issues of locomotion in granular matter. Peng *et al.* [11] extended the granular RFT for the case of a flexible filament; they considered different shapes of the filament and addressed issues such as maneuverability, change of direction, and changes in the filament size and geometry. In a subsequent study, the same group of researchers considered locomotion via the actuation of a flexible flapper [12]. Darbois Texier *et al.* [14] studied the motion of a rigid helix in granular media. In their case, the helix was driven by a shaft and it was possible to apply an external force to help or hamper the motion. They found the conditions for a force-free swim and proposed a model, also based on resistive force theory ideas but considering a simple Coulomb friction law. Given its similarity with the present study, some direct comparisons are drawn. The granular resistive force theory was recently shown to be amenable for proper scaling [15] and has also been proposed to model locomotion in granular media [16]. These recent findings are clear indications of the robustness of the granular RFT.

In this paper, inspired by the recent progress in the subject, we conduct experiments with helical swimmers in granular media to fully characterize this swimming strategy. In particular, the helical configuration allows us to simplify, somewhat, the swimming mechanics because the body shape remains fixed during the motion. Helical propulsion is used by bacteria such as *Escherichia coli* [17]. These organisms use the action of a rotatory helix to propel themselves in Newtonian fluids at low Reynolds numbers. This type of locomotion is relatively well predicted by the classical viscous RFT but there are more accurate methods such as the regularized Stokestlet method and Lighthill slender body theory [18]. These models indicate that the geometry of the helix is one of the most important parameters that affect the motion [19–23]. For the case of *E. coli*, the motion takes place at Reynolds numbers ranging between 10^{-5} and 10^{-4}, for which the inertial forces are negligible and viscous effects are dominant. For the case of dense granular matter the inertial force is also insignificant but, in turn, the frictional forces dominate. This fact is the basis for a fair comparison for swimming in these two media, despite the largely different scale of the swimmers. It is important to note that RFT has recently been shown to be more precise for granular materials than for Newtonian viscous fluids [16].

In a previous study, we used magnetically driven swimmers with helical tails in other complex fluids [24]. We use, essentially, the same system to produce self-locomotion of helical swimmers inside a bed of grains. In addition to varying the rotation speed of the helix, we widely vary its geometry. We also test the influence of particle size and roughness. The study is completed by adapting the granular RFT for helical swimmers, which leads to the identification of normalized variables. The results in this paper could be used to guide the design of autonomous robots capable of swimming in granular media. We envision that such devices could be used to tackle the problem of jamming in grain silos. The clogging of industrial silos is often resolved by sending workers inside these structures to manually clear the clogged regions in the silo. In many cases, the granular material can collapse on top of the workers, leading to severe injury or death. This is a serious industrial hazard, which has led to nearly 800 fatal and nonfatal accidents since 1964 in the United States alone [25]. Sending a robotic device instead would essentially eliminate the hazard.

II. EXPERIMENTAL SETUP AND PROCEDURE

To study swimming dynamics in sand we considered the self-propulsion of a magnetic robot. The swimmer, which consists of a magnetic head and a helical tail, was placed in a pool filled with particles located in the middle of rotating magnetic field. A rotating magnetic field device, designed by Godinez *et al.* [26], was used to impose a controlled rotation on the swimmer. Resulting from the interaction of the rotating helix with the granular media, the robot propelled itself without being attached to a shaft or any other external structure.

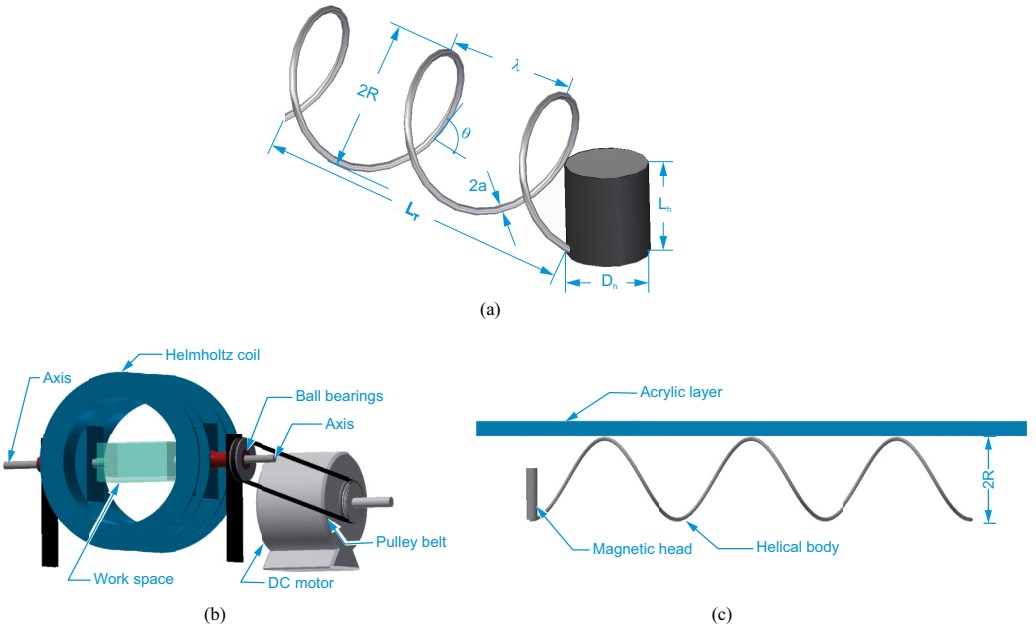

FIG. 1. (a) The head, where a permanent magnet is enclosed, has a diameter and length D_h and L_h, respectively. The helix can be characterized by its wavelength (λ), diameter ($2R$), helix angle (θ), and the thickness the spring ($2a$). (b) Scheme of the experimental setup. The work space is $70 \times 70 \times 140$ mm^3. (c) Configuration of the swimmer inside the granular matter with an acrylic plate on the top.

Several helical swimmers were designed and built inspired by geometry of the bacterium *E. coli* [17,27]. Figure 1(a) shows the schematic representation and the geometrical characteristics of the helical swimmer employed in the experiments. The swimmers were built with a cylindrical magnetic head with a diameter $D_h = 3.1$ mm and length $L_h = 7.0$ mm. The helix was made with stainless steel wire of thickness $2a = 0.51$ mm. In order to study the effect of the helix shape on the swimmer performance, several cases were considered by independently varying the helix angle (θ), the wavelength (λ), and the diameter ($2R$). Note that these geometrical properties of the helix are not fully independent since they are related by the relation $\tan\theta = 2\pi R/\lambda$.

As explained below, most experiments were conducted for the case for which the helix diameter was fixed, and the wavelength, λ, is varied (consequently, the pitch angle θ changes too). Table I shows the values of the geometric parameters of the first seven swimmers that were considered, which is referred to as case (i). Figure 2 shows a schematic view of these different helices. It is

TABLE I. Geometric parameters of the swimmers. Case (i): swimmers have the same diameter $2R$.

Swimmer	$2R$ (mm)	λ (mm)	θ (deg)	L_T (mm)	L_w (mm)
D11P6	11 ± 0.3	5.6	81.04	16.51	106.00
D11P12	11 ± 0.1	11.4	71.74	33.21	106.00
D11P20	11 ± 0.1	19.9	60.06	52.90	106.00
D11P29	11 ± 0.3	26.7	53.05	63.72	106.00
D11P41	11 ± 2.5	40.2	33.59	88.30	106.00
D11P60	11 ± 0.5	60.1	28.76	92.92	106.00
D11P95	11 ± 2.7	95.0	15.35	102.21	106.00

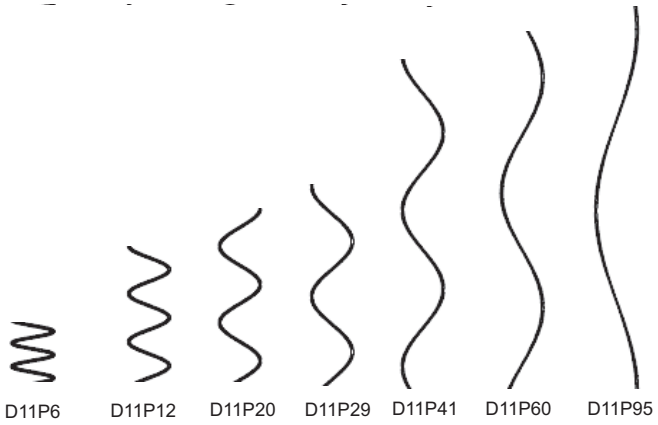

FIG. 2. The schematic representation for the seven swimmers employed in all experiments: case (i), constant $2R$. Note that the wire length in the helix, $L_w = L_t / \cos\theta$, is the same for all swimmers.

important to note that, to ensure a fair comparison among the swimmers, the total length of the tail, $L_w = L_T / \cos\theta$, was kept constant. This means that the same length of wire was used in all cases. The main results of this investigation were obtained for this set of swimmers.

To complete our study and to validate the proposed scaling (see Sec. III), we considered two additional groups of swimmers. In addition to case (i) presented above, we designed a group of swimmers with a fixed value of λ, but allowed θ and $2R$ to change [case (ii)]. A third group of swimmers [case (iii)] considered swimmers with a constant angle θ, allowing λ and $2R$ to change. The results for these additional cases are presented and discussed in Appendix B.

Granular media

The main set of experiments, where all the helical geometries were tested, was conducted with glass beads with a diameter of 0.375 ± 0.125 mm. The properties of this material are shown in Table II. The particles were relatively smooth, with an angle of repose $\gamma_o = 24.5^\circ \pm 1.5^\circ$. Figure 3(a) shows a typical image of the glass particles. The swimmer was placed on the surface of the medium and pushed down until it was completely covered by the beads reaching a depth of $2R$, as shown schematically in Fig. 1(c). To keep the swimmer immersed in the medium, an acrylic plate was placed on top of the granular pool. We did not find a significant influence of the plate on the swimming speed. Measurements with or without the plate and with plates with different roughness resulted in swimming speeds within the uncertainty of the measurement. Interestingly, when the plate was not used, the swimmer would tend to emerge from the granular bed. We attribute this flotation-like tendency to the static pressure gradient within the granular bed, but this behavior was not investigated further.

TABLE II. Properties of the granular media used in the experiments.

Type	Diameter (mm)	Angle of repose, γ_o (deg)	Density, ρ_p (kg/m^3)	Packing fraction
Glass	0.375 ± 0.125	24.5 ± 1.5	2500	0.60
Glass	0.6 ± 0.15	23.4 ± 1.8	2500	0.60
Glass	1.5 ± 0.15	23.8 ± 2.0	2500	0.59
Glass	2.0 ± 0.2	24.9 ± 1.8	2500	0.59
Glass	3.0 ± 0.25	25 ± 1.2	2500	0.58
Mustard	2.2 ± 0.29	32.4 ± 1.7	242.2	0.65

(a) (b)

FIG. 3. Photos of the particles used in this investigation as granular matter: (a) glass beads, 2.0 mm mean diameter; (b) mustard seeds, 2.2 mm mean diameter.

Once the swimmer was placed inside the granular matter, the coil was energized and rotated. When the magnetic field was strong enough, the swimmer rotated at the same rate as the coil and forward locomotion was observed. The horizontal displacement of the swimmer was recorded with a high-definition video camera and the images were analyzed with the software TRACKER 4.95. Experiments in which the rotation of the swimmer was not constant, and equal to the rotation rate of the external magnetic field, were discarded.

Two additional experimental campaigns were conducted. To test the influence of particle size, the swimmers of case (i) were tested with glass beads of four additional diameters: 0.6, 1.5, 2.0, and 3.0 mm (see Table II). A typical image of the glass particles is shown in Fig. 3(a). The angle of repose of these particle ensembles was approximately the same as for the 0.375 mm particles, indicating that they all had similar frictional properties.

To explore the influence of the material internal friction, a set of experiments was conducted using mustard seeds (see Table II), also with the case (i) swimmers. These particles had spheroidal shape and a very uniform size distribution. Figure 3(b) shows a typical image of the mustard seeds. Most notably, they have a larger angle of repose ($\gamma_o = 32.4^\circ \pm 1.7^\circ$), which results from having a rougher surface.

III. PREDICTIONS FROM GRANULAR RFT

As described in the introduction, Goldman and co-workers proposed a modified RFT model to calculate the speed of undulatory swimmers in a granular medium [7]. For this paper, we extend this idea for helical swimmers where the tail is a rigid helix that rotates at an imposed fixed rate.

The functional forms for the tangential F_T and normal forces F_N (per unit length) for a cylinder with radius a are

$$F_N = 2a(C_S \sin\beta_0 + C_F \sin\psi) \quad \text{and} \quad F_T = 2aC_F \cos\psi, \tag{1}$$

where ψ is the angle between the cylinder and the velocity vector. The angle β_0 relates the inclination of the cylinder with the frictional properties of the media by $\tan\beta_0 = \cot\gamma_0 \sin\psi$, where γ_0 is the angle of repose of the particulate media. The particle volume fraction ϕ, defined as the ratio of the volume occupied by grains to total volume, significantly affects the behavior of granular materials. The response of granular media to intrusion depends importantly on ϕ. Therefore, both C_S and C_F depend on ϕ [8]. In other words, C_S and C_F capture the compactness of the media, quantified by ϕ, and the internal slip angle, γ_0. Note that C_S and C_F have units of $\mathrm{kg/s^2}$.

The shape of the helix can be expressed as $\mathbf{r} = [x + V_x t, R\cos(kx - \omega t), R\sin(kx - \omega t)]$, where R is the outer radius of the helix, k is the wave number, ω is the rotational speed, and V_x is the helix velocity along the x direction. Considering that the inclination of the cylinder, ψ, is given by

$\sin\psi = V_N/\|V\|$, we can rewrite the normal and tangential forces as

$$F_N = \frac{2a}{\sqrt{V_x^2 + R^2\omega^2}}\left(\frac{C_S}{\sqrt{\sin^2\psi + \tan^2\gamma_0}} + C_F\right)V_N,$$
$$F_T = \frac{2aC_F}{\sqrt{V_x^2 + R^2\omega^2}}V_T, \tag{2}$$

where V_N and V_T are the normal and tangential velocities at the cylinder. Now, if we consider the helix to be composed of infinitesimal cylinders, we can project Eqs. (2) along the x direction. To obtain the total x force on the helix, we integrate

$$F_x = \int_0^{L_T} (F_T\,\hat{\mathbf{t}}\cdot\hat{\mathbf{e}}_\mathbf{x} + F_N\,\hat{\mathbf{n}}\cdot\hat{\mathbf{e}}_\mathbf{x})\,ds, \tag{3}$$

where L_T is the length of the helix, and $ds = dx/\cos\theta$, where θ is the helix angle. If we consider a self-propelled helix without a head, the speed, V_x, is found by setting the total force, F_x, to zero and solving the integral in Eq. (3). After some algebra, the normalized swimming velocity, $V_* = V_x/(\omega R)$, is expressed, in an implicit form, by

$$\begin{aligned} &V_*^4[\Gamma^2\tan^4\theta - \tan^2\theta\sec^2\theta - \sec^4\theta\tan^2\gamma_0] \\ &-2V_*^3[\Gamma^2\tan^3\theta + \tan\theta\sec^2\theta] \\ &+V_*^2[\Gamma^2\tan^2\theta\sec^2\theta - \sec^2\theta - \sec^4\theta\tan^2\gamma_0] \\ &-2V_*[\Gamma^2\tan^3\theta] + \Gamma^2\tan^2\theta = 0, \end{aligned} \tag{4}$$

where $\Gamma = C_S/C_F$. This equation can be solved numerically, for given values of R, ω, and θ, assuming that C_S and C_F are known. We used the two sets of values reported in Ref. [8], corresponding to low and high packing fractions. The predictions of this expression are shown below and contrasted with the experimental measurements. However, as shown in Fig. 1, the helices have a cylindrical head (through which the magnetic torque is applied) that is perpendicularly aligned to the mean motion. The head only adds drag and its effect can be readily incorporated into the expression above. The procedure is described in detail in Appendix A. Again, a fourth-order polynomial equation is found, similar to Eq. (4) but with additional terms corresponding to the drag on the head. Both predictions (with and without the head) are contrasted with the experimental measurements in the next section.

IV. EXPERIMENTAL RESULTS

The speed of helical swimmers, with different shapes inside different granular media, was measured experimentally. The behavior of the velocity for each swimmer for case (i) is presented in this section; results for cases (ii) and (iii) are shown in Appendix B.

A. The influence of helical geometry

We first present the experimental measurements, where the shape of the helix is varied but the particle type remains fixed. The experimental results of the swimming velocity are shown as a function of angular frequency, ω, and helix angle, θ, left and right, respectively, in Fig. 4.

Figures 4(a) and 4(b) show the swimming speed for the helical swimmers for which $2R$ is the same. For this case, the influence of the helix geometry can be observed clearly. The speed of the swimmer increases with ω. Since $2R$ is constant, the influence of θ and λ can be readily discerned. The robots D11P20 and D11P29 swam faster than the others, with values for λ of 19.9 and 26.7 mm, and for θ of 60.06° and 53.05°, respectively. This values correspond to the middle of the range. This, therefore, represents the optimal geometrical conditions to produce swimming. It is interesting to note that the robots D11P6 and D11P95 were the slowest ones: these two swimmers have opposite

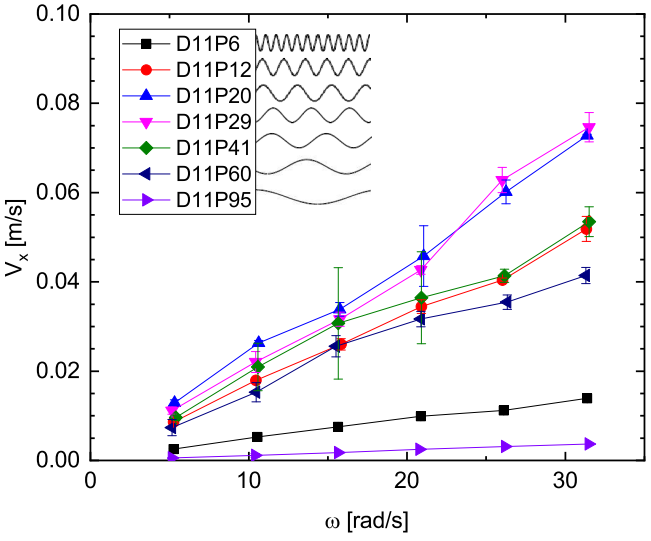

(a)

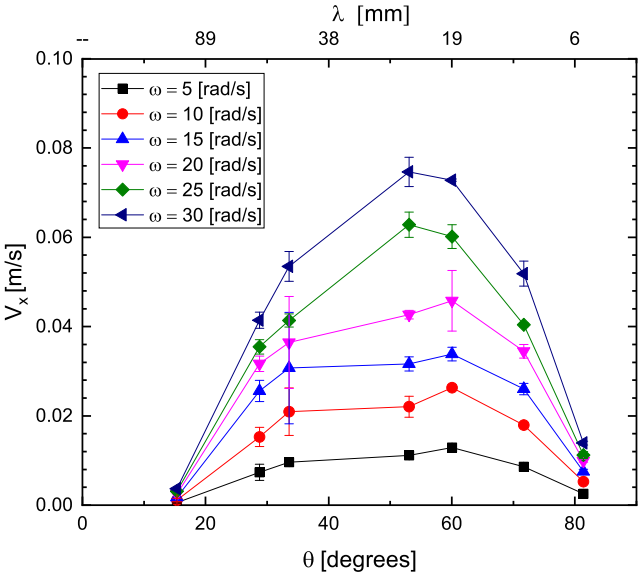

(b)

FIG. 4. Swimming speed for case (i) with glass particles of 0.325 mm in diameter. (a) Swimming speed as a function of rotational speed, ω. (b) Swimming speed as a function of helix angle, θ (also as a function of wavelength, λ). All data for swimmers with $2R$ constant.

values of the geometrical parameters (see Table I), having the largest and smallest θ values of this group, respectively. In Fig. 4(b), the influence of the helix angle is clearly shown. For a given rotational speed, a swimmer with an angle of about $\theta \approx 55^\circ$ swims fastest. This value is close to the middle of the range of the helix angle.

It is important to note that the swimmers with the smallest value of angle (swimmer D11P95, $\theta = 15.35^\circ$) hardly swam for any rotational speeds. It rotated freely but its forward motion was

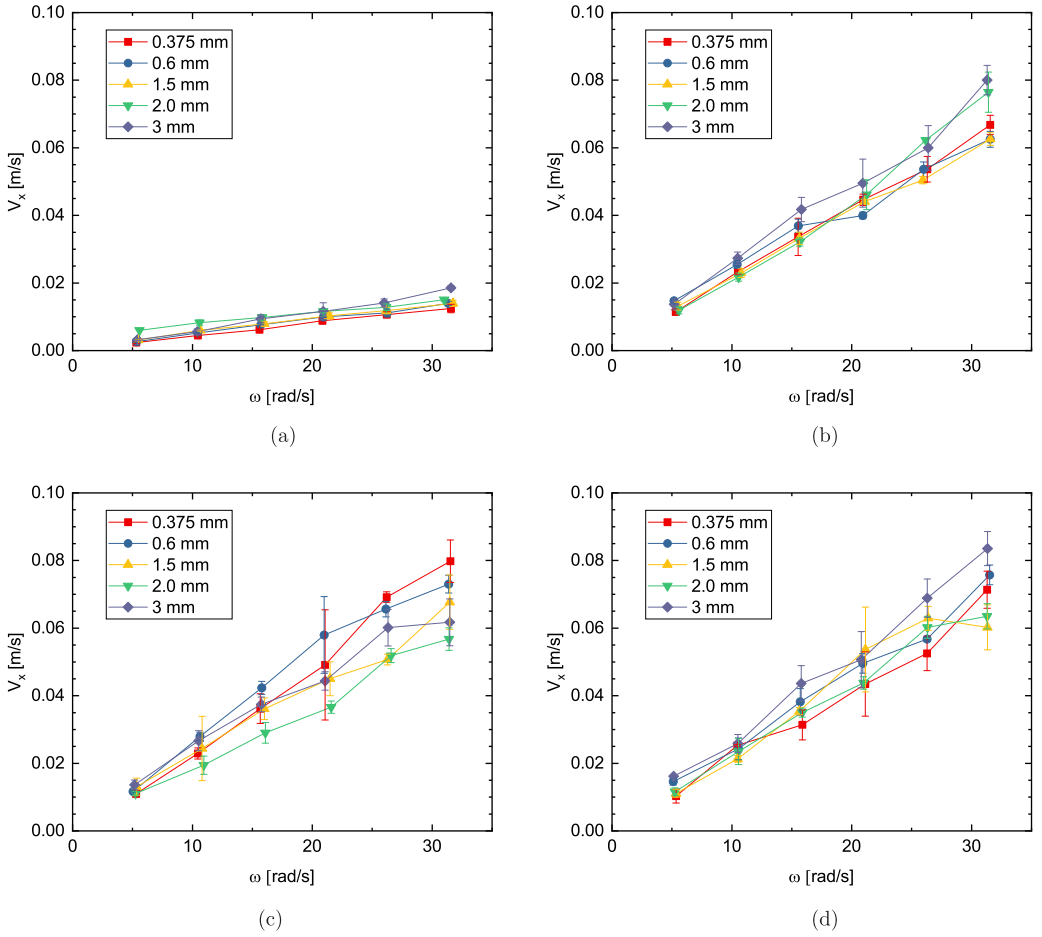

FIG. 5. Swimming speed as a function of rotational speed for different particle sizes. Each panel shows the results for different swimmers (see Table I): (a) D11P6, (b) D11P20, (c) D11P41, and (d) D11P60.

not significant even for long observation times. For the limiting cases (small or large θ), we do not expect to observe swimming. When the helix angle is close to 0°, the helix is essentially a straight cylinder; on the other hand, when the angle is close to 90° the helix becomes a hollow rod. For both of these cases, no net forward thrust can be produced. Two additional cases, which consider variations of the helix shape, were tested. The results were essentially the same as those presented above when considering normalized variables (see Sec. V). These data are shown in Appendix B.

B. Influence of particle size

The particle size has been recently identified as an important parameter in the generation of granular drag [6]. To evaluate the effect of particle size on the swimming speed, experiments were conducted with some of the swimmers for case (i) with glass particles of several sizes (see Table II). The results are shown in Fig. 5, where the swimming speed is shown as a function of rotational speed for five different glass particle sizes, with similar frictional properties. Despite the fact that the particle size is larger that the thickness of the coil, a, and even the size of the coil, R, the measured swimming speed is not significantly affected by the particle size. A slight increase in the

swimming speed is observed as particle diameter increases for all cases. For an increase of particle size of up to eight times, the swimming speed increases only 40% approximately.

C. Influence of grain internal friction

Since the internal friction of the material is a parameter that appears explicitly in the RFT model for swimming speed [Eq. (4)], it is interesting to conduct experiments for grains with different values of the angle of repose. The swimmers of case (i) were tested in mustard seeds. As shown in Table II, this material has a mean particle diameter of 2.2 mm, which is close to one of the glass particles used. Most importantly, since mustard seeds are rougher [see Fig. 3(b)], their angle of repose is larger than that of glass spheres.

These results appear in Fig. 6, where the swimming speed is shown as a function of the angular rotation speed (on the left) and as a function of the helix angle (on the right). Since the particle size did not have a significant influence on the swimming speed (as shown in the previous section), these speeds can be directly contrasted with those shown in Figs. 4(a) and 4(b). The same qualitative trend is observed with the mustard seeds: the speed increases with angular frequency and there is an optimal angle of the helix that maximizes speed (around 50°). One important difference found for this type of grain is that the swimming speed is smaller (in comparison with the glass beads), for all cases. The reduction is approximately 40% with respect to the glass sphere tests. Clearly, the swimming speed decreases as the angle of repose increases.

V. DISCUSSION

From the results shown above, we can attempt to find scalings and identify the parameters that affect the swimming speed. From classical resistive force theory, and also from its granular form described in Sec. III, the forward thrust arises from the rotation of the helix. Specifically, the swimming speed increases linearly with ωR. For clarity, only the results from case (i) are discussed since the other two cases essentially convey the same information.

Figures 7(a) and 7(c) show the speed measurements for case (i) normalized by ωR, for glass beads and mustard seeds, respectively. The data clearly collapse into a single band, indicating that the speed indeed scales with ωR. Presented in this manner, it is clear that there is an angle at which the speed is maximized, at around 55° for both particle types. The value $V_x/\omega R$ represents the relationship between the forward speed and the tangential speed at the edge of the helix. Note that the normalized results of cases (ii) and (iii) also fall into the same band of data (shown in Appendix B), which further demonstrates the robustness of the scaling.

Another way to analyze the results is to calculate the wave efficiency [13]. Essentially, the swimming speed is compared with the wave speed $\omega\lambda$. A value of $V_x/(\omega\lambda)$ close to 1 would indicate the motion of a screw penetrating perfectly through an undeformable media. In other words, the swimmer would move as fast as the wave induced by the helical shape. Figures 7(b) and 7(d) show the normalized speeds considering $\omega\lambda$ for the glass particles and mustard seeds, respectively. The results also collapse nicely into a single band of data. This is not surprising since it was shown that the speed scaled with ω (since R is fixed in this case). The new scaling does show a more robust scaling of the data since λ does vary for each swimmer. The swimming wave efficiency for all experiments is below 15%, slightly smaller for the case of mustard seeds. More importantly, the normalization with $\omega\lambda$ shows a maximum value at a different angle, in comparison with the ωR normalization. In this case, the angle at which the wave efficiency has a maximum value is close to 70° for both types of particles.

Comparison with predictions from RFT

As discussed above, it is possible to find an implicit equation to determine the swimming speed of a helical swimmer in a granular medium. The model essentially takes the ideas described in Ref. [7] to calculate both thrust and drag over the swimmer. We extend this idea for the case of a rigid

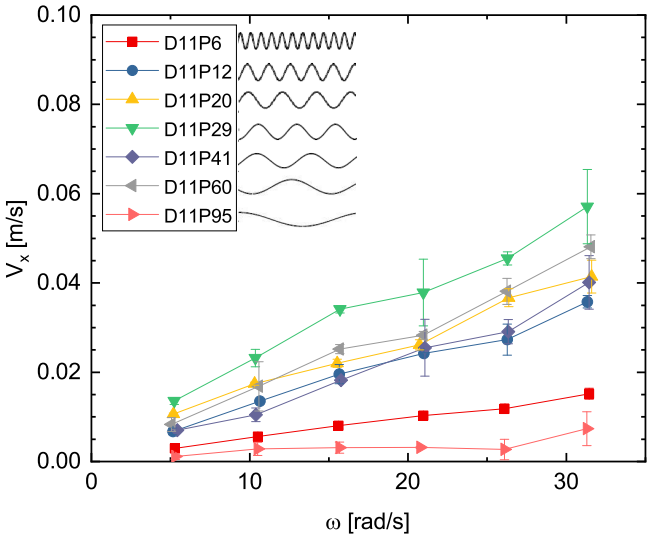

(a)

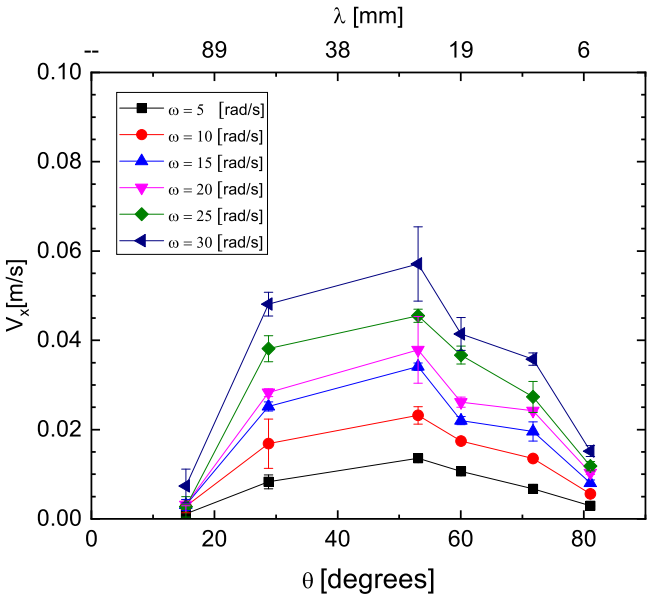

(b)

FIG. 6. Swimming speed for mustard seeds. On (a), the speed is plotted as a function of rotational speed; on (b), the swimming speed is shown as a function of helix angle. Case (i) swimmers are tested. The properties of the grains are shown in Table II.

helical tail. The model indicates that, in agreement with the experimental results, the swimming speed scales with ωR. Additionally, the swimming speed is also affected by the helix angle, θ, the angle of repose of the material, γ_o, and the ratio Γ, as shown by Eq. (4).

Figure 8 shows the direct comparison between the measured velocities for swimmers of case (i) for both glass particles and mustard seeds. Note that the model predictions do consider the effect of the head [Eq. (A2)]. A value of $\Gamma = 1.82$ was used considering the low packing fraction

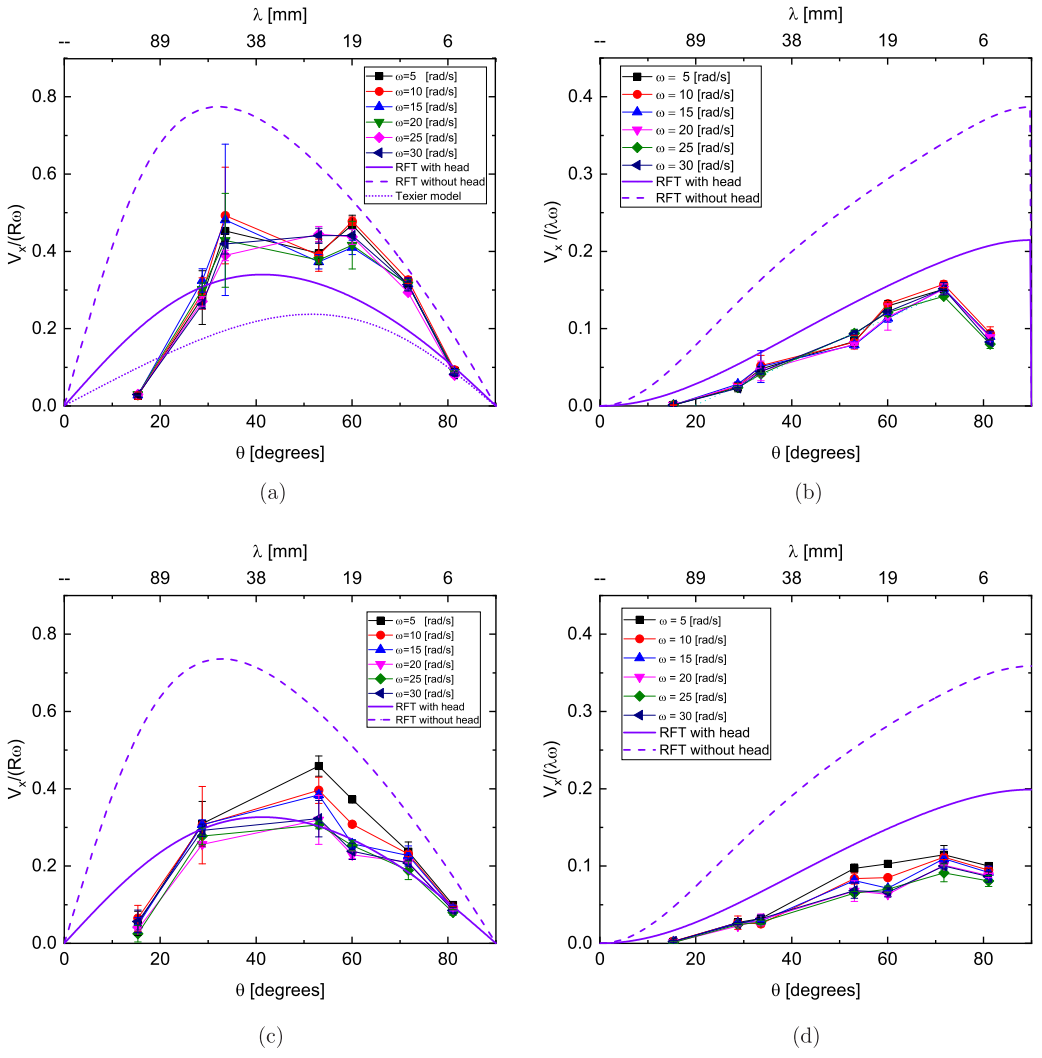

FIG. 7. Normalized speed as a function of the angle for all swimmers in case (i). On the left [(a) and (c)] the speed is normalized with ωR, while on the right [(b) and (d)] the normalization is done with $\omega\lambda$. The lines are the predictions from granular resistive force theory: the solid lines show the model with the head [Eq. (A2)]; the dashed lines show the predictions without the effect of the head [Eq. (4)]. The dotted line in (a) shows the model prediction from Ref. [14]. (a) and (b) Glass particles and (c) and (d) Mustard seeds.

condition from Ref. [8]. The experimental measurements and the predictions agree very well, both qualitatively and quantitatively. They both show a linear increase of speed with ω and the existence of an angle for which the speed is a maximum. The prediction underestimates the experimental results, for about 30% but only for large helix angles, for glass spheres. Another important difference between the measurements and the predictions is that the angle for maximum speed is different. While experimentally, the angle is around 55°, for the model the angle is about 30°. The model also does predict that the swimming speed is smaller for a higher angle of repose, in accordance with experiments.

For the lines shown in Fig. 8 we used the values of Γ reported in Ref. [8]. By considering Γ to be a free fitting parameter we can make the predictions match the experiments more closely. For the glass beads and mustard seeds we found that $\Gamma = 0.989$ and $\Gamma = 2.454$, respectively, give the best

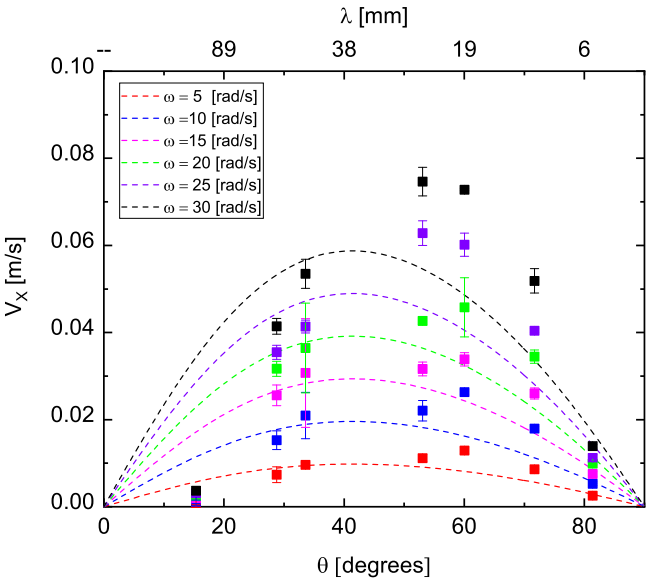

(a)

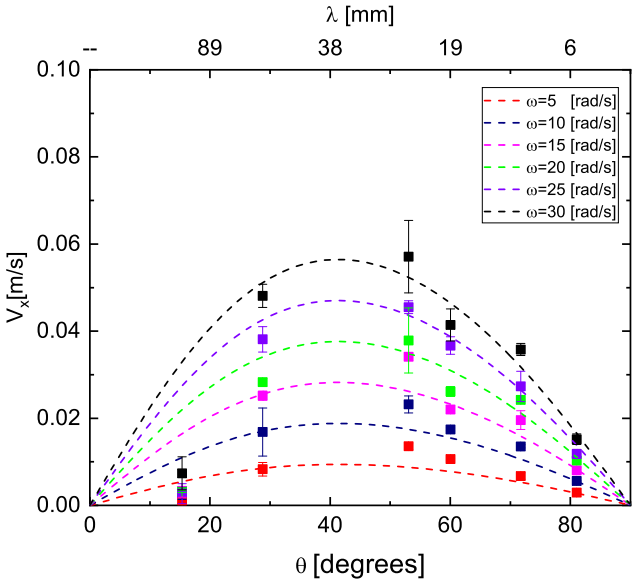

(b)

FIG. 8. Speed as a function of helix angle, θ, and wavelength, λ, for different rotation speeds. The lines show the predictions from Eq. (A2), which does account for the presence of the head. Each color, both symbols and lines, corresponds to different values of the angular speed, ω. (a) Glass particles and (b) Mustard seeds.

fit. For clarity these lines are not shown. These values are different from those reported in Ref. [8] but retain the same order.

Since the scaling with ωR (or $\omega\lambda$) shows a good collapse of the experimental results, it is natural to conduct comparisons with normalized variables. The model, as shown in Eqs. (4) and (A2), scales with ωR. The lines in Fig. 7 show the predictions from the models with and without the head

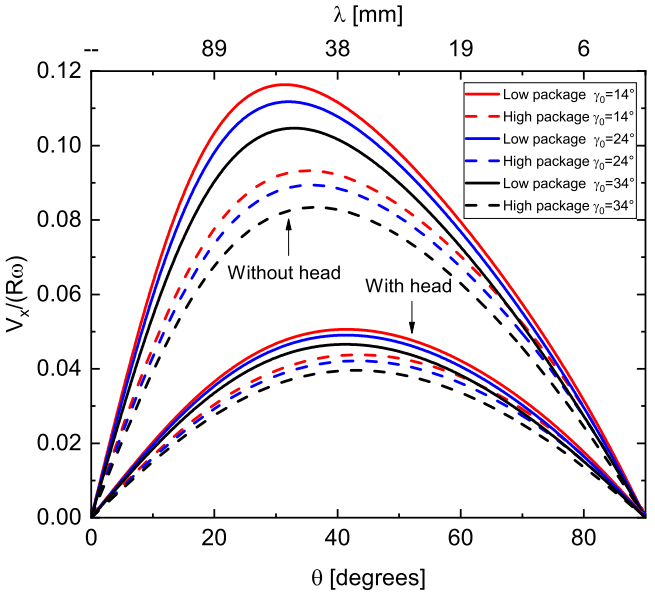

(a)

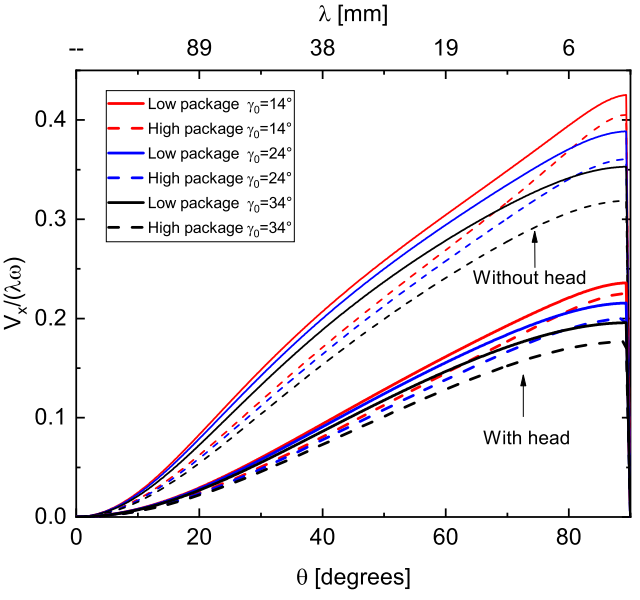

(b)

FIG. 9. (a) Speed as function of helix angle, θ, and (b) wavelength, λ. Predictions from the RFT model [Eqs. (4) and (A2)]. Predictions for two values of Γ, low packing (dashed lines) and high packing (solid lines), and for three values of the angle of repose.

[Eqs. (A2) and (4), respectively]. When the effect of the head is not accounted for, the prediction is slightly above the experimental measurements, as expected. When the effect of the head is considered, the difference between the measurements and predictions is within 15%. The main difference between the experiments and the model predictions (for the normalization with ωR) is

the angle at which the maximum speed is attained. For the normalization with $\omega\lambda$, the experimental measurements do show a maximum but the model seems to predict a nonzero value for $\theta = 90^\circ$. For the wave efficiency, the predictions of the model are slightly above the experimental measurement but they do capture the progressive increase of wave efficiency as the angle increases. The angle for which the maximum wave efficiency is observed experimentally is not reproduced by the model predictions.

We can also compare our results with the model predictions from Darbois Texier *et al.* [14], for the case of a force-free swimmer. In such a case, the normalized speed is given by

$$\frac{V_x}{\omega R} = \frac{C_n/C_t - 1}{\tan\theta + \frac{C_n/C_t}{\tan\theta}}, \tag{5}$$

where C_n and C_t are normal and tangential drag coefficients. Considering that $C_n/C_t = 1.6$ (obtained by following their calculation method for the parameters in our experiment), a prediction can be readily obtained and contrasted with the present results. The dotted line in Fig. 7(a) shows the prediction from this model. Although their model agrees with several features of the present results, the value of the normalized speed is smaller, despite the fact that the drag on the head is not accounted for. Including the effect of the head would lead to an even smaller prediction. Nevertheless, the prediction is relatively close to the experimental measurements. One important aspect of the prediction in Ref. [14] is that the angle of the helix at which the maximum velocity is obtained appears to be closer (in comparison with our RFT model prediction) to that obtained experimentally. Considering a ratio of $C_n/C_t = 2.7$ the model predictions match the experiments well. Again, this value is different from that reported in Ref. [14] but the difference is not large.

Finally, given the good agreement between the model and the experiments, we can now vary the value of different parameters in the model to investigate their effect on the prediction. In fact, an explicit solution can be obtained for Eq. (4) by analytically solving the fourth-order polynomial equation; however, its solution is rather impractical. Therefore, we opted to obtain the solution using the software MATHEMATICA. One disadvantage of this strategy is that the effect of the different parameters is not evident. In Fig. 9 the predictions of the model are shown in terms of $V_x/\omega R$ and the wave efficiency (left and right, respectively). There are several groups of lines: the thick and thin lines correspond to the cases when the head is accounted for or neglected, respectively. Clearly, the general behavior is the same: since the head only adds drag, the normalized speeds decrease when the effect of the head is accounted for. The continuous lines (of three different colors) show the effect of varying the angle of repose of the material. The model predicts a decrease of the swimming speed for an increasing angle of repose, γ_o, which agrees with the experimental trend shown above. Last, since the model is constructed from the fact that the values C_S and C_F are known and constant, it is interesting to change their value. We considered the measurements of Maladen *et al.* [7] for the low and high packing fraction of grains, leading to two values of $\Gamma_{LP} = 1.85$ and $\Gamma_{HP} = 1.05$. When the value of Γ is decreased, corresponding to a more compacted state, the swimming speed is reduced. Note that a smaller value of Γ indicates less drag anisotropy, which reduces the ability of the helix to produce thrust, leading to a reduced speed. The value of packing was not varied in the experiments performed here; hence, it is not possible to draw comparisons.

VI. CONCLUSIONS

The motility of free helical swimmers in granular media is studied experimentally. The geometrical characteristics of the swimmer robots, which represent an advantage in swimming ability, were obtained. In addition to the rotational speed, ω, the swimming speed is affected by the values of λ and θ (or R). The particle roughness was found to reduce the swimming speed, but this parameter was not varied widely. In contrast, changing the particle size widely did not seem to affect the swimming speed significantly. The extension of the granular RFT theory to consider the rigid helical tail produced a model for which predictions showed a good agreement with our experimental data. The model only had a free parameter, Γ. The model also captured several

other features of the experiments, but two important aspects were not captured. The first aspect involves the minimum conditions for motion and the angle at which the velocity is a maximum. We found that, for small angles of the helix, the swimmer rotates around its axis, but does not move forward. It appears that an angle threshold should exist. Second, the experiments showed that a helix angle of approximately 55° results in a maximum normalized speed; in contrast, the granular RFT predicts a smaller angle for the fastest swimming (about 30°). The wave efficiency appears to reach a maximum experimentally, at around 70°, but the model prediction does not show such maximum efficiency. The reasons for these differences remain to be resolved. The present experimental campaign contributes to the current discussion on locomotion in granular media and further validates the granular RFT modeling.

ACKNOWLEDGMENT

R. Valdés and V. Angeles greatly acknowledge the support of CONACyT-Mexico during their Ph.D. studies.

APPENDIX A: MODEL FOR A SWIMMER WITH A CYLINDRICAL HEAD

To compare the prediction with the experiments in a quantitative manner, the effect of the swimmer's head needs to be included. The swimmer, as shown in Fig. 1, has a cylindrical head (through which the magnetic torque is imposed) that is perpendicular to the mean motion. Therefore, the force balance, Eq. (3), is modified by adding the drag force on the head, F_h, as

$$F_x = \int_0^{L_T} (F_T\,\hat{\mathbf{t}}\cdot\hat{\mathbf{e}}_\mathbf{x} + F_N\,\hat{\mathbf{n}}\cdot\hat{\mathbf{e}}_\mathbf{x})ds + \int_0^{L_h} F_h dx, \tag{A1}$$

where $F_h = F_N \sin\theta_h - F_T\cos\theta_h$. In our case, the head is a cylinder of length L_h with its axis aligned perpendicular to the swimmer's main movement, in x; hence, $\theta_h = 90°$. RFT considers that the flagellum is, in fact, a collection of small cylinders. For this reason we can use the similar modeling to account for the drag on the head considering an additional contribution of F_N and F_T accounting for the differences in size. Therefore, the main differences to model the head drag are that the diameter of the cylinder is $D_h/2$ (instead of $2a$) and the length is L_h. Also, the inclination angle of the head cylinder, θ_h, is 90°. Considering the new force balance [Eq. (A1)] and expressions for the tangential and normal forces (2), an implicit expression for V_x, including the effect of the head, can be written as

$$\begin{aligned}
&V_*^4\{\Gamma^2\tan^4\theta - \tan^2\theta\sec^2\theta - \sec^4\theta\tan^2\gamma_0\\
&\quad - 2L_*\sec\theta[\Gamma^2\tan^3\theta - \tan^2\theta - \sec^2\theta\tan^2\gamma_0] - L_*^2[\tan^2\theta - \Gamma^2\sec^2\theta + \sec^2\theta\tan^2\gamma_0]\}\\
&\quad - 2V_*^3\{\Gamma^2\tan^3\theta + \sec^2\theta\tan\theta - L_*\tan\theta\sec\theta[2+\Gamma^2] + L_*^2\tan\theta\}\\
&\quad + V_*^2\{\Gamma^2\tan^2\theta\sec^2\theta - \sec^2\theta - \sec^4\theta\tan^2\gamma_0\\
&\quad - 2L_*\sec\theta[\Gamma^2\tan^2\theta + 1 + \sec^2\theta\tan^2\gamma_0] + L_*^2[\Gamma^2\sec^2\theta - \sec^2\theta\tan^2\gamma_0 - 1]\}\\
&\quad - 2V_*[\Gamma^2\tan^3\theta + L_*\Gamma^2\tan\theta\sec\theta] + \Gamma^2\tan^2\theta = 0,
\end{aligned} \tag{A2}$$

where

$$L_* = \frac{L_h}{L_T}\frac{D_h}{2a}. \tag{A3}$$

It is important to note that Eq. (4) is recovered if L_* is set to zero.

Equation (A2) is also solved numerically using MATHEMATICA to obtain the the speed V_x, following the same procedure as for Eq. (4).

TABLE III. Geometric parameters of the swimmers: case (ii), swimmers have constant λ; case (iii), swimmers have the same helix angle θ.

	Swimmer	$2R$ (mm)	λ (mm)	θ (deg)	L_T (mm)	L_w(mm)
Case (ii)	D5P20	4.2	20 ± 0.3	33.2	100.00	127.15
	D8P20	8.2	20 ± 0.1	51.76	78.70	127.15
	D11P20	10.5	20 ± 0.3	58.39	66.64	127.15
	D17P20	16.6	20 ± 0.01	68.73	46.13	127.15
Case (iii)	D5P6	5.5	6.6	70 ± 0.91	18.88	52.90
	D7P8	7.0	7.7	70 ± 0.70	17.48	52.90
	D9P10	11.0	12.2	70 ± 0.49	17.66	52.90
	D11P13	12.0	11.9	70 ± 2.45	15.92	52.90
	D15P14	14.9	14.1	70 ± 3.22	15.26	52.90

APPENDIX B: EXPERIMENTAL RESULTS FOR CASES (ii) AND (iii)

Two additional cases were tested to observe the influence of helix geometry on the locomotion. Case (i), presented above, considers the situation when $2R$ is approximately constant at 11 ± 2.7 mm but λ and θ change. For case (ii) we consider a fixed value of $\lambda = 20 \pm 0.3$ mm, but θ and $2R$ change. Finally, for case (iii), the angle θ is kept constant, at around $70^\circ \pm 3.2^\circ$. For these two additional cases the total wire length ($L_T / \cos\theta$) was also kept constant to ensure a fair comparison among

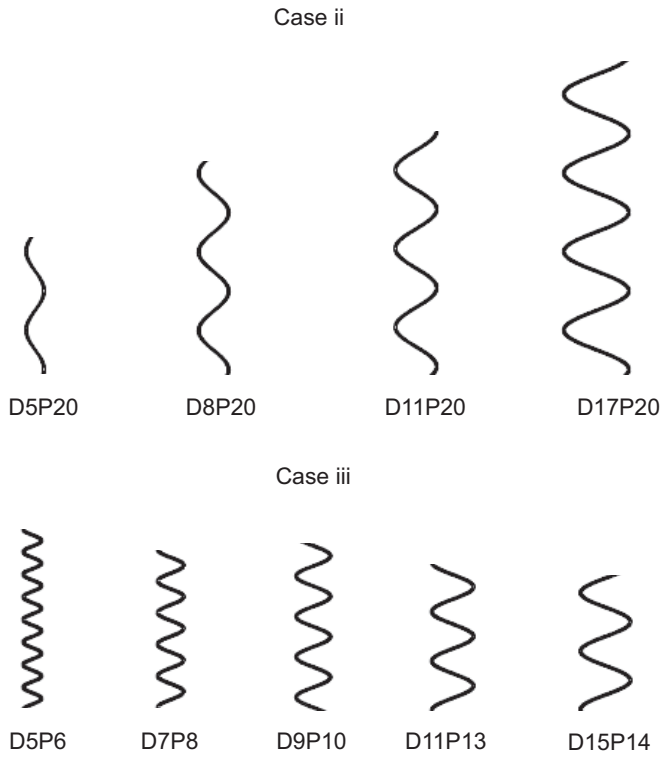

FIG. 10. The schematic representation for the nine swimmers employed in all experiments. Case (ii), constant λ; case (iii), constant θ. Note that the wire length is the tail; $L_w = L_t / \cos\theta$, is constant for each case.

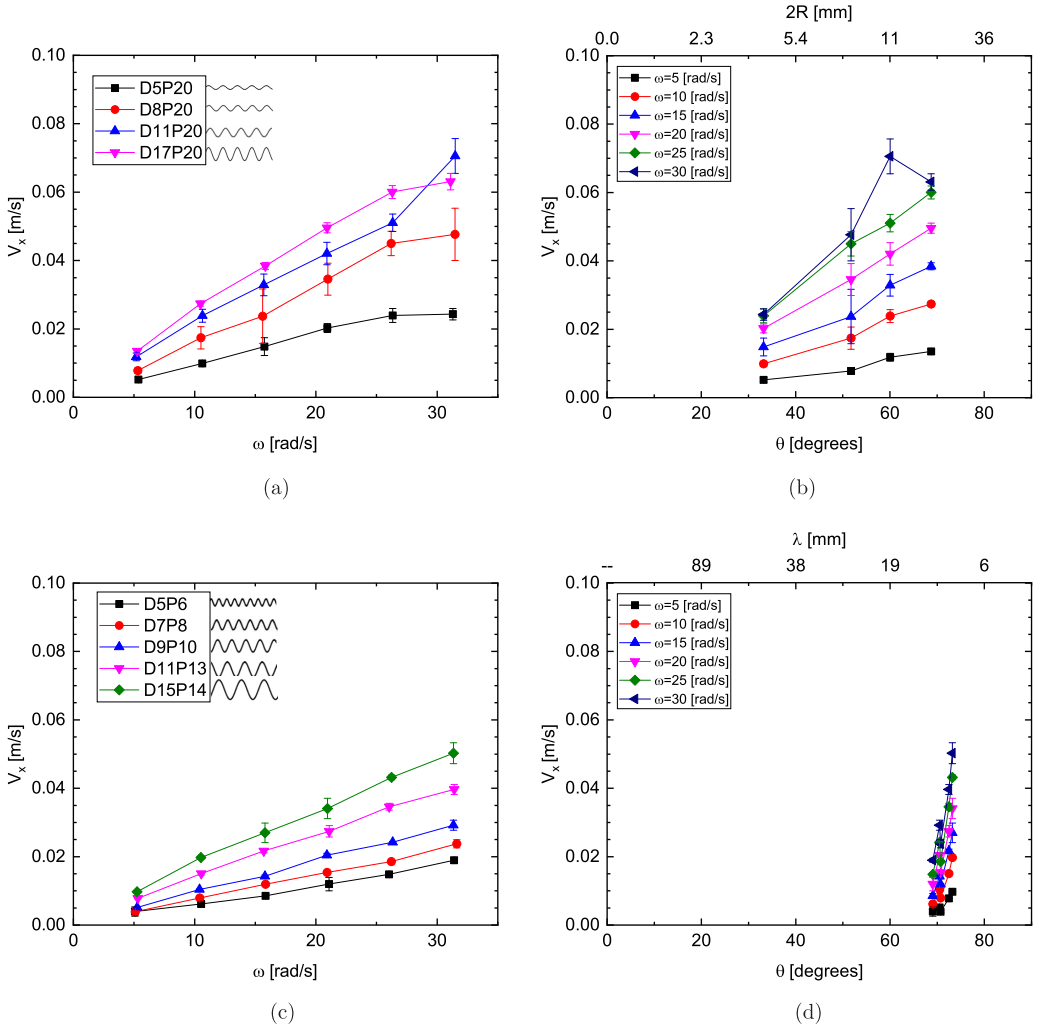

FIG. 11. Swimming speed for cases (ii) and (iii) with glass particles of 0.325 mm in diameter. On the left and right columns, the swimming speed is shown as a function of the rotational speed, ω, and the helix angle, θ (or alternatively as a function of wavelength λ or helix size $2R$). (a) and (b) Case (ii) λ is constant and (c) and (d) Case (iii) θ is constant.

the swimmers. The values of the parameters used for the swimmers are shown in Table III and a schematic view is shown in Fig. 10.

1. Case (ii): Constant λ

Figures 11(a) and 11(b) show the velocity of swimmers for which λ is constant, but θ and $2R$ change, as shown in Table I. For a given shape (a given robot), the swimming speed increases with rotational speed, ω. For a given rotational frequency, the swimming speed increases with helix angle, θ. Note that in this case, the helix angle spans only from 35° to 70°.

The swimmer D17P20, which has the largest angle and the largest radius (see Fig. 2), swam faster than the others. In contrast, the swimmer D5P20 had the smallest velocity of this group of swimmers. This behavior can be related to the values of θ and $2R$. For large values of the angle and the radius, the robot swims faster.

2. Case (iii): Constant θ

Figures 11(c) and 11(d) show the swimming speed of five different swimmers inside the granular medium with conditions listed in Table I. In this case the helix angle is kept constant, but R and λ change. This case is interesting because, since the helix angle is fixed, the shape of the helix is simply scaled in size. As in case (i), the swimming speed increases with ω. It can be seen in Fig. 11(c) that the swimming speed increases with R. The speed increased progressively from robot D5P6 to robot D15P14 (the smallest and largest values of R, respectively). Since the angle is constant, Fig. 11(d) does not convey any significant information.

[1] S. Childress, *Mechanics of Swimming and Flying*, Cambridge Studies in Mathematical Biology (Cambridge University Press, Cambridge, UK, 1981).

[2] T. Wei, R. Mark, and S. Hutchison, The fluid dynamics of competitive swimming, Annu. Rev. Fluid Mech. **46**, 547 (2014).

[3] A. E. Hosoi and D. I. Goldman, Beneath our feet: Strategies for locomotion in granular media, Annu. Rev. Fluid Mech. **47**, 431 (2015).

[4] T. Shimada, D. Kadau, T. Shinbrot, and H. J. Herrmann, Swimming in granular media, Phys. Rev. E **80**, 020301(R) (2009).

[5] Y. Forterre and O. Pouliquen, Flows of dense granular media, Annu. Rev. Fluid Mech. **40**, 1 (2008).

[6] K. Kamrin, Quantitative rheological model for granular materials: The importance of particle size, in *Handbook of Materials Modeling: Applications: Current and Emerging Materials* (Springer International, New York, 2018), Chap. 1, pp. 1–24.

[7] R. D. Maladen, Y. Ding, C. Li, and D. I. Goldman, Undulatory swimming in sand: Subsurface locomotion of the sandfish lizard, Science **325**, 314 (2009).

[8] R. D. Maladen, Y. Ding, P. B. Umbanhowar, A. Kamor, and D. I. Goldman, Mechanical models of sandfish locomotion reveal principles of high performance subsurface sand-swimming, J. R. Soc. Interface **8**, 1332 (2011).

[9] T. N. Zhang and D. I. Goldman, The effectiveness of resistive force theory in granular locomotion, Phys. Fluids **26**, 101308 (2014).

[10] R. D. Maladen, P. B. Umbanhowar, Y. Ding, A. Masse, and D. I. Goldman, Granular lift forces predict vertical motion of a sand-swimming robot, in *2011 IEEE International Conference on Robotics and Automation* (IEEE, Piscataway, NJ, 2011), pp. 1398–1403.

[11] Z. Peng, O. S. Pak, and G. J. Elfring, Characteristics of undulatory locomotion in granular media, Phys. Fluids **28**, 031901 (2016).

[12] Z. Peng, Y. Ding, K. Pietrzyk, G. J. Elfring, and O. S. Pak, Propulsion via flexible flapping in granular media, Phys. Rev. E **96**, 012907 (2017).

[13] J. Gray and G. J. Hancock, The propulsion of sea-urchin spermatozoa, J. Exp. Biol. **32**, 802 (1955).

[14] B. Darbois Texier, A. Ibarra, and F. Melo, Helical Locomotion in a Granular Medium, Phys. Rev. Lett. **119**, 068003 (2017).

[15] J. Slonaker, D. C. Motley, Q. Zhang, S. Townsend, C. Senatore, K. Iagnemma, and K. Kamrin, General scaling relations for locomotion in granular media, Phys. Rev. E **95**, 052901 (2017).

[16] H. Askari and K. Kamrin, Intrusion rheology in grains and other flowable materials, Nat. Mater. **15**, 1274 (2015).

[17] H. C. Berg, *E. coli in Motion* (Springer, New York, 2004).

[18] B. Rodenborn, C. H. Chen, H. L. Swinney, B. Liu, and H. P. Zhang, Propulsion of microorganisms by a helical flagellum, Proc. Natl. Acad. Sci. USA **110**, E338 (2013).

[19] T. Atsumi, Y. Maekawa, T. Yamada, I. Kawagishi, Y. Imae, and M. Homma, Effect of viscosity on swimming by the lateral and polar flagella of Vibrio alginolyticus, J. Bacteriol. **178**, 5024 (1996).

[20] M. Shigematsu, A. Umeda, S. Fujimoto, and K. Amako, Spirochaete-like swimming mode of *Campylobacter jejuni* in a viscous environment, J. Med. Microbiol. **47**, 521 (1998).
[21] J. G. Mitchell, The energetics and scaling of search strategies in bacteria, Am. Nat. **160**, 727 (2002).
[22] B. R. Robertson, J. L. O'Rourke, B. A. Neilan, P. Vandamme, S. L. On, J. G. Fox, and A. Lee, *Mucispirillum schaedleri* gen. nov., sp. nov., a spiral-shaped bacterium colonizing the mucus layer of the gastrointestinal tract of laboratory rodents, Int. J. Syst. Evol. Microbiol. **55**, 1199 (2005).
[23] E. Lauga and T. R. Powers, The hydrodynamics of swimming microorganisms, Rep. Prog. Phys. **72**, 096601 (2009).
[24] S. Gomez, F. Godínez, E. Lauga, and R. Zenit, Helical propulsion in shear-thinning fluids, J. Fluid Mech. **812**, R3 (2017).
[25] S. Riedel and B. Field, 2010 summary of grain entrapments in the United States, Technical report, Purdue University, 2011 (unpublished).
[26] F. A. Godínez, O. Chavez, and R. Zenit, Note: Design of a novel rotating magnetic field device, Rev. Sci. Instrum. **83**, 066109 (2012).
[27] S. Chattopadhyay, R. Moldovan, C. Yeung, and X. L. Wu, Swimming efficiency of bacterium Escherichia coli, Proc. Natl. Acad. Sci. USA **103**, 13712 (2006).